# Chapter 6

# *The Force-Matching Procedure: A Civil Engineering Application*

**The following papers (by Liut *et al.*) are based on the contents of the this chapter:**

- **"Neural-Network Control of Building Structures," (reference [51])**
- **"An overview of Some Non-Traditional Neural-Network Training Strategies for Seismic Response Suppression of Building Structures," (reference [56])**
- **"Neural-Network Control of Building Structures by a Force-Matching Training Scheme," (reference [58])**

## 6.1 Introduction

In this chapter we discuss a new technique to train a neural-network controller in order to reduce the response of a building excited by earthquakes. The controller utilized is a tuned mass damper (TMD) located on the roof of the building. These devices give a good response reduction when working in passive mode. The main goal of the active neural-network controller is to optimize the performance of the already efficient passive tuned mass damper.

During the training process, the neural-network weights are gradually modified until the desired output is achieved. One of the methods used to train neural networks is the backpropagation technique. As we explained in Chapter 4, this technique is easy to implement when the target behavior of the neural network is known. It requires the determination of the gradient of an appropriate performance measure of the system with respect to the neural-network weights. The performance measure of the system is defined in terms of the difference between the current and the desired outputs. The gradient information is used for updating the neural-network weights. In the context of control of dynamic structural response, the objective of a neural-network-based controller is to generate control actions (forces) such that they cause a desired reduction in the response. In such a case, the input to the controller consists of some of the measured response quantities such as displacements, velocities, and accelerations of the structure, as well as some characteristics of the excitation.

If the control forces required to produce the desired structural response were known, we could straightforwardly train the neural network to generate such forces by means of the backpropagation technique. But in structural control applications, the desired controller output (*i.e.*, the required control force) is unknown beforehand. Thus a direct application of this approach is not feasible for such case. For the application we discuss in this chapter this means that when a building structure is subjected to a seismic excitation, the control forces that would minimize the structural response are unknown beforehand and therefore the backpropagation technique cannot be applied straightforwardly.

One way to circumvent this problem is to represent or *emulate* the structural system by a separate neural network for which the performance-function gradients can be easily obtained. This emulator neural network is trained prior to training the neural-network controller, and it is used as a neural interface between the controller and the set of output state variables that are to be reduced by the control actions. To train the neural-network emulator, a suitable norm of the difference between the outputs of the actual building (or

a model of it) and of the emulator for a set of disturbances, is minimized. This strategy, thus, requires two neural networks: one to generate efficient control actions, and another to emulate the structural system. This approach was first adopted by Narendra and Parthasarathy [71] and Nguyen and Widrow [76] in the application of neural networks to dynamical systems. In the field of earthquake engineering applications, Faravelli and Venini [21], Chen *et al.* [10], Bani-Han *et al.* [1], and Joghataie and Ghaboussi [37] have successfully utilized this approach.

In this chapter an alternative training approach, herein called the force-matching technique [51, 56, 58], is applied. It does not require the emulation of the structure by an additional neural network. The basis of the force-matching procedure is similar to the moment-matching procedure we described in Chapter 5. In addition to speeding up the calculations, this approach can eliminate some of the approximations and uncertainties embedded in the emulation stage mentioned above. The proposed approach is implemented on a shear-beam model of a multi-story structure controlled by an active tuned mass damper, as the one described in Chapter 3.

A relevant issue in the development of neural-network-based controllers is the choice of the input data set to be used during the training process. For seismic-response reduction, the ideal situation would be to train the neural-network controller with the earthquake motions the structure would encounter during its life span. This is obviously impossible, as future earthquakes cannot be known. However, it is reasonable to expect that future seismic events will posses similar site-specific spectral characteristics in an average sense. Thus, a set of input training earthquakes is defined by an ensemble of synthetically generated time histories, which are consistent with a predefined site spectrum. To demonstrate the effectiveness of the neural network trained with such input data, the system is subjected to two recorded earthquakes that were not part of the training data set.

## 6.2 The Neural-Network Controller and the Structural Model

For our work, we use a two-layer neural network controller like the one we described in Chapter 4. A schematic of it is shown in Figure 6-1. Here we summarize the equations that represent this neural network for each layer:

Layer *I*:

$$v_j^I(t) = \sum_{i=1}^{N^0} w_{ji}^I \; p_i(t) \qquad \text{for} \quad j = 1,\ldots, N^I \tag{6.1}$$

$$y_j^I(t) = A^I \tanh\left(\beta^I v_j^I(t)\right) \qquad \text{for} \quad j = 1,\ldots, N^I \tag{6.2}$$

Layer *II*:

$$v^{II}(t) = \sum_{j=1}^{N^I} w_j^{II} \; y_j^I(t) \qquad \text{for} \quad j = 1,\ldots, N^I \tag{6.3}$$

$$u_c(t) = A^{II} \tanh\left(\beta^{II} \; v^{II}(t)\right) \tag{6.4}$$

where **p** is the input vector, $N^0$ is the dimension of vector **p**, $N^I$ is the number of neurons of the first layer, $w_{ji}^I$ are the weights of the first layer, the hyperbolic tangents represent the squashing functions, $w_j^{II}$ is the single set of weight coefficients for to the second layer, and $u_c$, is the output of the neural network, which is the control command. The constants $A^I$ and $\beta^I$, for the first layer, and $A^{II}$ and $\beta^{II}$, for the second layer, are parameters of the neural network. In both cases they are tuned heuristically.

We use the neural-network controller to command the control actions to generate the control forces for a TMD located on the top level of a multi-story building, as described in Figure 6-3. The final goal is to reduce the structural response to a seismic excitation. To model the building, we use the linear structural description discussed in Chapter 3, which can be summarized as follows:

$$\mathbf{M}\,\ddot{\mathbf{z}}(t) + \mathbf{C}\,\dot{\mathbf{z}}(t) + \mathbf{K}\,\mathbf{z}(t) = \mathbf{M}\,\mathbf{r}\,\ddot{x}_g(t) + \mathbf{h}\,u(t) \tag{6.5}$$

where **z** is the $N_d \times 1$ vector of relative displacements of each degree of freedom with respect to the base, $N_d$ is the number of degrees of freedom of the building-TMD system $(N_d = number\ of\ floors + 1)$, the acceleration $\ddot{x}_g$ is the seismic excitation, the $N_d \times N_d$ matrices **M**, **C** and **K**, are the mass, damping and stiffness matrices of the system, respectively, the $N_d \times 1$ vector **r** is the influence vector of the ground motion, and **h** is the $N_d \times 1$ location vector, which specifies the position of the actuator.

The following frequency, mass, and damping ratios, described in Chapter 3, account for the characteristics of the tuned mass damper:

$$f_r = \frac{\omega_a}{\omega_1}; \quad m_r = \frac{m_a}{m_t}; \quad \xi_a = \frac{c_a}{2\,m_a\,\omega_a} \tag{6.6}$$

where $m_a$, $k_a$ and $c_a$, are the mass, stiffness and viscous damping coefficients of the TMD, $\omega_a$ and $\omega_1$ indicate the fundamental frequencies of the TMD and the structure, respectively, and $m_t$ is the total mass of the building.

## 6.3 Training the Neural Network

If the desired output $u_d$ of the controller were known, the supervised backpropagation procedure, as described in Chapter 4, could be implemented. However, for structural control applications, $u_d$ is usually not known in advance: it is precisely the function to be determined in order to achieve the desired objective (response reduction). What is known is the desired response of the structural system to be controlled. The question arises, then, if this error can be expressed in terms of the desired and calculated structural responses. Figure 6-2.*a* presents a schematic of the neural network controller and the structural system. The feedback inputs and outputs are also shown in this figure. Figure 2.*b* depicts a possible evolution trend of the error $e$ defined in terms of the desired and calculated control force, whereas Figure 2.*c* shows the error $e_r$ defined as the difference between some desired and computed structural responses. The proposed training approach relies on being able to establish a relationship between the response difference $e_r$ and the control error $e$ such that any action (during the training process) that reduces $e_r$ also reduces $e$. This requires that: (1) $|e_r(k)|$ be equal to or larger than $|e(k)|$, and (2) $e_r(k)$ and $e(k)$ have the same signs during the training process. The argument $k$ is the time step. These conditions will ensure that the two errors move in the same direction, and if the larger one approaches its desired zero value then the smaller one will also approach that value. In the next section we discus how, under certain conditions, it is possible to establish such an upper bound for the control error $e(k)$ in terms of the acceleration response of a suitable floor of the structure. This procedure avoids the need for developing an additional neural network to represent the structure as mentioned in the first section.

Our goal is then to find a suitable backpropagation error $e_r$ that bounds the error $e$ representing the difference between the desired control force and the actual force computed by the neural-network controller. Since the error $e$ is the difference between two forces, an error $e_r$ expressed in terms of the acceleration response of the structure seems to be a suitable error estimator. Indeed, we found that the inertial accelerations of

the building provide a good estimate of this error signal under certain conditions. This leads to the proposed force-matching technique.

## 6.4 The Force-Matching Training Procedure

The approach introduced here seeks to reduce the response of a seismically excited multi-story building by means of the control force generated by a tuned mass damper as described in the last section (see Figure 6-3).

To reduce the response, the control actions seek to reduce the lateral inertial forces on the structure as much as possible. For a lumped-mass model of the structure, this objective can be formulated as the problem of minimizing an instantaneous performance index defined as:

$$\hat{\Psi}(k) \cong \sum_{i=1}^{N_f} \left| \ddot{z}_i^a(k) \right| \tag{6.7}$$

where $k$ is the current time step, $N_f$ is the number of floors and $\ddot{z}_i^a$ stands for the absolute acceleration of the $i^{th}$ floor, given by,

$$\ddot{z}_i^a(k) = \ddot{z}_i(k) + \ddot{x}_g(k) \tag{6.8}$$

The control law applied to the TMD is defined through an appropriate selection of the neural-network weights. The objective is to obtain a set of weights that defines a control law, which minimizes $\hat{\Psi}$ for all time. The appropriate values of the weights are obtained through successive small adjustments by means of the backpropagation technique as we explained in Chapter 4. Each adjustment of the weights causes a change $\Delta u_c$ in the actuation force, which in turn leads to a reduction in the controlled response. If the optimal actuation $u_d$ were known for all time, $\Delta u_c$ would be given by

$$\Delta u_c(k) = u_d(k) - u_c(k) \tag{6.9}$$

A small change in the control actions, $\Delta u_c$, is associated with small reductions in the lateral accelerations of the structure, $\Delta \ddot{z}_i$ . They are related as follows

$$\Delta u_c(k) = \sum_{i=1}^{N_f} m_i \Delta \ddot{z}_i(k) \tag{6.10}$$

where the small higher order changes in the damping and stiffness related forces associated with the small time training step used during the integration process as well as the effect of the small forces associated with relatively small tuned mass damper parameters are ignored. Based on equation (6.10), we can write the following inequality:

$$\left|\Delta u_c(k)\right| \le \sum_{i=1}^{N_f} m_i \ \left|\Delta \ddot{z}_i(k)\right| \tag{6.11}$$

The training technique described in this section requires certain conditions to be satisfied. In order to guarantee that the successive adjustments performed to the control law generate a smooth reduction of the building response, the training algorithm should produce gradual improvements in the actuations, such that their effect on the building structure always satisfies

$$\left|\Delta \ddot{z}_i(k)\right| \le \ \left|\ddot{z}_i(k)\right| \tag{6.12}$$

$$\text{sign}\left[\Delta \ddot{z}_i(k)\right] = -\text{sign}\left[\ddot{z}_i^a(k)\right] \tag{6.13}$$

for $i = 1, \ldots, N_f$. Equation (6.13) prescribes that, if the magnitude of the acceleration of a certain floor mass is to be reduced, the change in the acceleration produced by the control action must have the opposite sign of the corresponding floor acceleration. Equation (6.12) implies that this change must be less than the current acceleration in order to avoid overcompensation, thus allowing for a gradual reduction of the magnitude of the acceleration. By considering Equations (6.11) and (6.12), the following inequality is obtained:

$$\left|\Delta u_c(k)\right| \leq \sum_{i=1}^{N_f} m_i \left|\ddot{z}_i^a(k)\right| \tag{6.14}$$

Additional conditions regarding the characteristics of the building response are still required by the proposed training technique to generate an effective control action. In particular, we assumed that the lateral acceleration pattern, at least for most of the duration of the earthquake, is such that the magnitudes of the floor accelerations increase from the base of the building to its top; that is:

$$\left|\ddot{z}_j^a(k)\right| \leq \left|\ddot{z}_i^a(k)\right| \tag{6.15}$$

$$\text{sign}\left|\ddot{z}_j^a(k)\right| = \text{sign}\left|\ddot{z}_i^a(k)\right| \tag{6.16}$$

for $i \geq j$. For a building structure this is equivalent to expecting a predominantly first-mode acceleration response. During an actual earthquake event, such conditions may not hold for all time. Nevertheless, the training technique performed efficiently in all cases explored. The dynamic response of a typical building subjected to a seismic excitation will usually have a dominant first-mode contribution, thus satisfying conditions (6.15) and (6.16) most of the time. Also, since the TMD is tuned close to the fundamental

period of the structure, the force applied through it has the tendency to enforce these conditions.

As long as conditions (6.15) and (6.16), regarding the acceleration response, are satisfied, the following inequality also holds:

$$\sum_{i=1}^{N_f} m_i \left| \ddot{z}_i^a(k) \right| \leq m_t \left| \ddot{z}_{\max}^a(k) \right| \tag{6.17}$$

where $m_t = \sum_{i=1}^{N_t} m_i$ is the total mass of the building and $\ddot{z}_{\max}^a$ stands for the maximum instantaneous lateral acceleration, which is given by the top floor acceleration, for a structure vibrating predominantly in the first mode. We can define a new inequality consistent with inequality (6.17) in terms of any floor *k* as follows:

$$\sum_{i=1}^{N_f} m_i \left| \ddot{z}_i^a(k) \right| \leq \gamma_n \; m_t \left| \ddot{z}_n^a(k) \right| \tag{6.18}$$

where $\gamma_n \geq 1$ is a parameter that depends on the location of the floor level *n*. This parameter represents the ratio between the instantaneous acceleration values at the top and $n^{th}$ floors. Substituting the last inequality into inequality (6.14), it follows that,

$$\left| \Delta u_c(k) \right| \leq \gamma_n \; m_t \left| \ddot{z}_n^a(k) \right| \tag{6.19}$$

This expression defines an upper bound for the instantaneous absolute value of the control correction $\Delta u_c$ or the (preliminary) backpropagation error $e(k)$.

Next we consider the relation between the signs of $\Delta u_c$ and the floor accelerations. Equations (6.12) and (6.13) express the conditions that the improvements on the control actions must produce if they are to introduce gradual improvements to the acceleration

profile. Also, we have assumed that the acceleration distribution pattern is described by equations (6.15) and (6.16) for most of the duration of the seismic event. Therefore, considering Equations (6.10), (6.13) and (6.16) we can write the desired sign of the control force increment in terms of the sign of the instantaneous acceleration corresponding to the $n^{th}$ floor as follows:

$$\text{sign}\left|\Delta u_c(k)\right| = -\,\text{sign}\left|\ddot{z}_n^a(k)\right| \tag{6.20}$$

This implies that the force correction must have the effect of reducing the lateral acceleration of the structure.

The two expressions (6.19) and (6.20) constitute the basis for the definition of an approximate training error $e_r(k)$ as follows:

$$e_r(k) = -\,\gamma_n\; m_t\; \ddot{z}_n^a(k) \tag{6.21}$$

We can now implement the backpropagation training approach with $e_r(k)$ as the error estimator. This estimator depends on the absolute acceleration of a particular story $n$. During the numerical simulations, it was found that not all of the lateral accelerations provide equally effective estimations of the real backpropagation error $e(k)$. For example, the lateral accelerations of stories immediately close to the last story did not produce good training-error estimations. The strong influence of the TMD actuator in this region of the structure may constitute the main reason for this. Something similar can be said of the lateral accelerations close to the ground, where the earthquake excitation has a strong influence. In general, we found that the acceleration corresponding to a floor level $n$ at about 70-80% of the building height constitutes an efficient training error signal.

In a convergent training process, the error indicator would go to zero as the optimal response is approached. This optimal response ideally corresponds to a zero-acceleration response. However, it is not practically possible to reduce all lateral accelerations to zero

for all time. Consequently the backpropagation algorithm based on the error $e_r(k)$ may not lead to a convergent result. Therefore, it is necessary to introduce some additional criterion to detect when a practical level of response reduction has been achieved, to stop or modify the training process, and to limit an indefinite growth in the network weights.

To achieve this, constraints on some of the actuation parameters are introduced. We explored limitations based on the level of the mechanical power, control force, and velocity of the actuator, with similar control results for these options. Such limitations can be imposed by modulating the backpropagation error signal as follows,

$$\hat{e}_r(k) = e_r(k)\,\mu(k) \tag{6.22}$$

where $\mu$ is defined as:

$$\mu(k) = \tanh\left[\beta_p\,|\Delta\chi(k)|\right] \tag{6.23}$$

and

$$\Delta\chi(k) = \frac{\chi_{\max} - |\chi(k)|}{\chi_{\max}} \tag{6.24}$$

Here $\chi(k)$ is an actuator variable to be limited (such as the power, force, or velocity), $\chi_{\max}$ is its limiting reference value, and $\beta_p$ is a tuning constant. As $\chi$ approaches $\chi_{\max}$, $\mu$ makes the absolute value of the error smaller. Thus $\mu$ plays the role of a dynamic learning parameter, which slows down the learning process when the instantaneous value of the variable $\chi(k)$ approaches its limiting reference value. With the error modulation described in equation (6.22), and taking into account equation (6.21), the sensitivity function defined in Chapter 4 are now modified as follows:

$$\hat{\delta}_j^I(k) = w_j^{II}(k)\,\hat{\delta}^{II}(k)\,\frac{\partial y_j^I}{\partial v_j^I}(k) \tag{6.25}$$

$$\hat{\delta}^{II}(k) = -\gamma_n\ m_t\ \ddot{z}_n^a(k)\,\mu(k)\,\frac{\partial y^{II}}{\partial v^{II}}(k) \tag{6.26}$$

In conjunction with this error modulation, an additional heuristic procedure is implemented to limit the final magnitude of the weight values. This procedure is based on the concepts borrowed from the Instar, Outstar and Kohonen rules, currently applied in neural-network-based pattern recognition (see Hagan, [26]). These rules seek to prevent the weights from growing without bound by introducing some restrictions as they get larger. A decay term is introduced, which is proportional to each weight in each of the three rules. The decay term is also proportional to the input to the neural network in the case of the Instar rule, and to the output from the neural network in the case of the Outstar rule. The Kohonen rule adopts the value of the learning parameter to be the same as the value of the decaying rate parameter. The concepts embedded in these three rules are used to propose the following new rule for a multi-layer neural network:

- If $|\chi(k)| \le \chi_{\max}$ then

$$\begin{aligned} \Delta w_{ji}^I(k) &= \lambda^I\ \hat{\delta}_j^I(k)\ p_i(k) \\ \Delta w_j^{II}(k) &= \lambda^{II}\ \hat{\delta}^{II}(k)\ y_j^I(k) \end{aligned} \tag{6.27}$$

- If $|\chi(k)| > \chi_{\max}$ then

$$\begin{aligned} \Delta w_{ji}^{I}(k) &= -\text{sign}\left(w_{ji}^{I}(k)\right) \left| \lambda^{I} \hat{\delta}_{j}^{I}(k)\ p_i(k) \right| \\ \Delta w_{j}^{II}(k) &= -\text{sign}\left(w_{j}^{II}(k)\right) \left| \lambda^{II} \delta^{II}(k)\ y_j^{I}(k) \right| \end{aligned} \tag{6.28}$$

Thus, according to Equation (6.28), when $|\chi(k)| > \chi_{\max}$ the magnitudes of the current weights are only decreased by the magnitudes of $\Delta w_{ji}^{I}(k)$ and $\Delta w_{j}^{II}(k)$.

## 6.5 Numerical Results

The numerical evaluation of the proposed controller is carried out using a 10-story shear building model. A schematic of this model is shown in Figure 6-3. The mass and stiffness properties of the structure are uniform along the height of the building. The first natural period is about 1 *sec*. A modal damping ratio of 3% is assumed for all modes to define the damping matrix of the system. As we have discussed, the building is equipped with an active TMD acting on the top floor. Its characteristic parameters are given by: $f_r = 0.91$, $m_r = 0.04$, and $\xi_a = 0.10$.

We explored two different control configurations: 1) acceleration-feedback, 2) velocity-feedback. For the case of acceleration feedback, the input to the controller consists of the absolute floor acceleration plus the collocated actuator stroke and velocity. For the velocity-feedback case, the input vector consists of the velocities of each floor relative to the base plus the collocated stroke and velocity of the actuator. Thus, in both cases, the total number of input quantities is 12; that is, $N^0 = 12$. The neural-network architecture (Figure 6-1) consists of 8 neurons in the first layer and one neuron in the second layer; that is $N^I = 8$, and $N^{II} = 1$. To start the training process, the weight initialization is done with small random numbers.

We use a set of 10 artificially-generated earthquakes, with spectra compatible with a given response spectrum, as the training input data. The same set of earthquakes is used several times, but each time their sequential order is randomly shuffled at the beginning of each cycle to avoid any undesired bias during the training process. After the training is completed, the controller design is evaluated using two different seismic records, which were not included in the training set. The records used for validation are the El Centro (1941) and San Fernando (1971) ground-acceleration time histories, normalized to a maximum peak acceleration of $0.3\,g$. The spectra for these two time histories are shown in Figure 6-4 along with the average spectrum of the earthquake time histories used in the training set, all obtained for 3% damping.

We first discuss the results for the acceleration-feedback controller. The base shear forces (a force quantity of design interest) for the El Centro and San Fernando seismic motions are shown in Figures 6-5.*a* and 6-5.*b*, respectively. The base shear values have been normalized with respect to the weight of the building. The thicker lines represent the response for the controlled case; the thin lines represent the same for the uncontrolled case. It is observed that the controller produces significant response reductions for both earthquake inputs (49% for El Centro earthquake and 41% for San Fernando earthquake) in spite of their dissimilar characteristics apparent in the uncontrolled responses and their response spectra. In Figures 6-6.*a* and 6-6.*b* we show the required control forces normalized with respect to the weight of each floor, for both earthquakes. For both motions, the peak control force is about 0.13 of the floor weight, although the overall control requirement is larger in the El Centro case. Similar characteristics of the control demand can also be noticed in the corresponding peak values of the TMD stroke, as shown in Figures 6-7.*a* and 6-7.*b*, which reach the values of $0.42\,m$, and $0.30\,m$, for the El Centro and San Fernando cases, respectively.

The next set of three figures is for the velocity-feedback controller. They are parallel to Figures 6-5, 6-6 and 6-7 described in the previous paragraph for the acceleration-feedback scheme. Figures 6-8.*a* and 6-8.*b* show the controlled and uncontrolled base-

shear responses for the El Centro and San Fernando cases, respectively. It is seen that the peak values of the responses are reduced by about 53% (slightly better than acceleration feedback) for the El Centro motion and 35% (slightly worse than acceleration feedback) for the San Fernando motion. Figures 6-9.*a* and 6-9.*b* show the time history of the control force, normalized with respect to a floor weight. The peak values are now 16% and 12% of the floor weight for the El Centro and San Fernando cases, respectively, compared to 13% in the acceleration-feedback case. The time variations of the TMD stroke for the two excitation cases are shown in Figure 6-10.*a* and 6-10.*b*. The maximum stroke lengths required are $0.33\,m$ and $0.31\,m$ for the El Centro and San Fernando motions, respectively. These are smaller than the corresponding values in the acceleration-feedback case mentioned in the previous paragraph. Again it is observed that, from the standpoint of the level of control effort, the El Centro earthquake is a more demanding seismic event than the San Fernando event; the controller plays a more important role in the latter case, producing greater response reductions, but of course at the expense of increased force and stroke. It is relevant to observe that even though these results for the velocity-feedback case are not very different from the corresponding acceleration-feedback results, the peak mechanical power required by the velocity-feedback controller is only about 40% of that required by the acceleration-feedback controller. This suggests that the velocity-feedback controller performs more efficiently than its acceleration-feedback counterpart, at least in this case.

In Table 6-1 the control effectiveness of the acceleration and velocity-feedback schemes for the two earthquake motions are compared. The peak values for the relative displacement, interstory drift and absolute acceleration responses at different levels of the building are shown. They represent the ratios of the controlled to corresponding uncontrolled peak responses. Thus, a smaller value implies a larger reduction in the response. For a better comparison of the results obtained in the two feedback cases, the maximum actuator power level is kept at about the same level in the two cases. The upper part of the table is for the El Centro motion and the lower part for the San

Fernando motion. The results for the passive operation of the TMD $(u = 0)$ are shown. For a better visual comparison, these results are also plotted in Figures 6-11.*a*, 6-11.*b*, 6-12.*a*, 6-12.*b*, 6-13.*a*, and 6-13.*b*. In each case, part *a* of the figure is for the El Centro earthquake and part *b* for the San Fernando earthquake. From these results, we can see that the velocity- feedback controller is in general more effective than the acceleration-feedback controller. Both the El Centro and San Fernando earthquakes exhibit an increase in the interstory drift close to the top of the building. Since the drift is a measure of the lateral structural forces, and the present model of the building has the same stiffness and geometrical characteristics along its structure, this increase in the intersory drift near the top of the building is directly related to the strong influence of the active TMD in this region. From the standpoint of practical feasibility, the acceleration-feedback scheme seems more appropriate, since acceleration measurements can be made more easily than the relative velocity measurements. But some recent laser-based measurement devices, even if currently more expensive than simple accelerometers, are making it quite convenient to measure relative velocities as well.

The next two figures display the special nonlinear features of the neural-network controller. Figures 6-14.*a* and 6-14.*b* show the response reduction factors for the base shear and top-floor acceleration responses for various levels of ground excitations. We can see that the neural-network controller is effective for a large range of ground motion intensity $(0.1\,g \text{ to } 1.0\,g)$ for both events, with only a slight degradation in the control effectiveness for higher intensities. The results shown in these figures correspond to the velocity-feedback controller. In these two figures the response reduction factors corresponding to the TMD device acting in passive mode $(u = 0)$ is also shown. This allows us to compare the effectiveness of the active control system with respect to the passive case. The corresponding control requirements are shown in Figure 6-15, which shows the normalized value of the peak control force as a function of the peak ground acceleration, for both El Centro and San Fernando earthquakes. From this figure it follows that the control force required for the higher levels of excitations to achieve a

certain level of response reduction does not increase linearly with the intensity of the excitation. As the peak ground acceleration increases, the corresponding control force seems to approach a saturation limit.

## 6.6 Concluding Remarks

In this chapter we adapted the load-matching training technique introduced in Chapter 5 for a naval application, to a force-matching procedure for a civil engineering application. We used this procedure to train a neural-network controller in order to minimize the response of a structure under seismic excitations. This approach does not require an additional neural-network to emulate the structure as commonly demanded by other backpropagation-based schemes. We used a set of synthetically generated ground motions to train the controller, and two historic ground acceleration records (El Centro and San Fernando) to evaluate the controller performance and validate the training process. We want to emphasize that these two earthquakes were not part of the training set. The training process proved efficient and expeditious. We experimented with two different controller implementations corresponding to acceleration- and velocity-feedback schemes. In both cases the resulting controller exhibits a good performance, with significant response reductions and feasible control requirements.

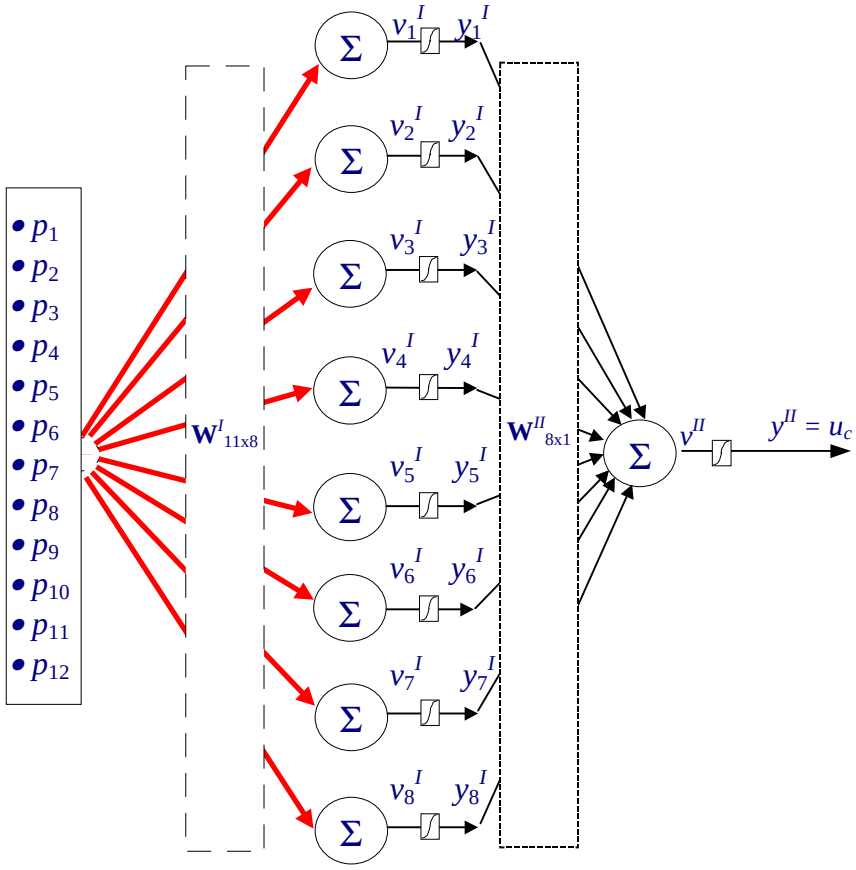


Figure 6-1: Nine-neuron, two-layer neural-network controller used in this work. Thick arrows account for different sets of weighted input data.

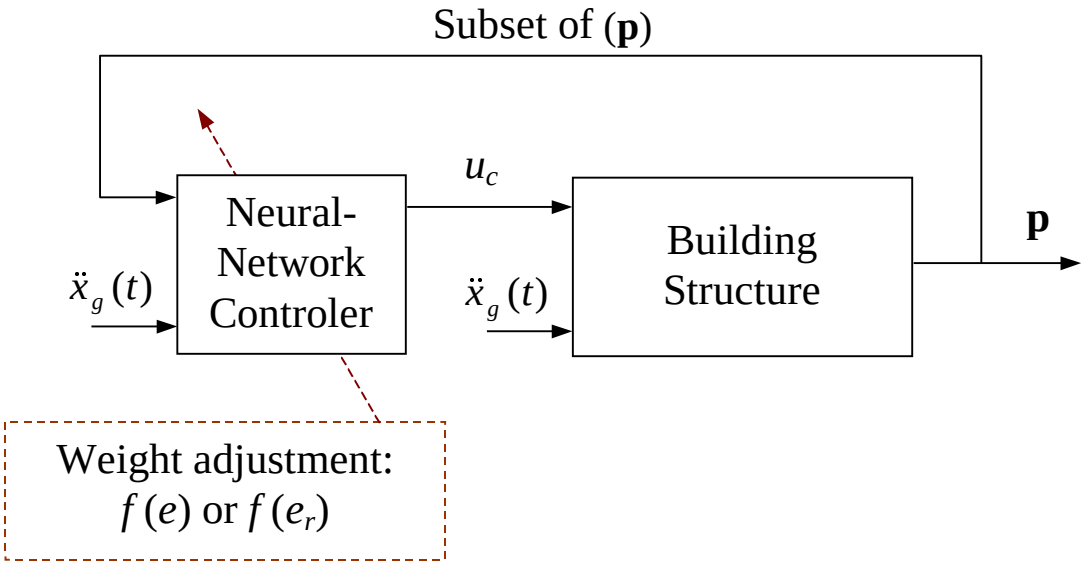


(a)

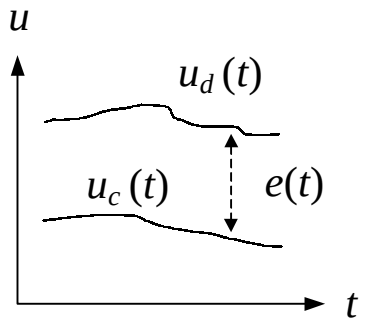


$$e(t) = u_d(t) - u_c(t)$$

(b)

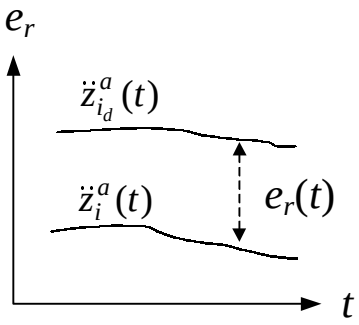


$$e_r(t) = \ddot{z}^a_{i_d}(t) - \ddot{z}^a_i(t)$$

(c)

Figure 6-2: (a) Neural-network and building schematic, (b) evolution of the controller error, and (c) evolution of the acceleration response error of floor *i*.

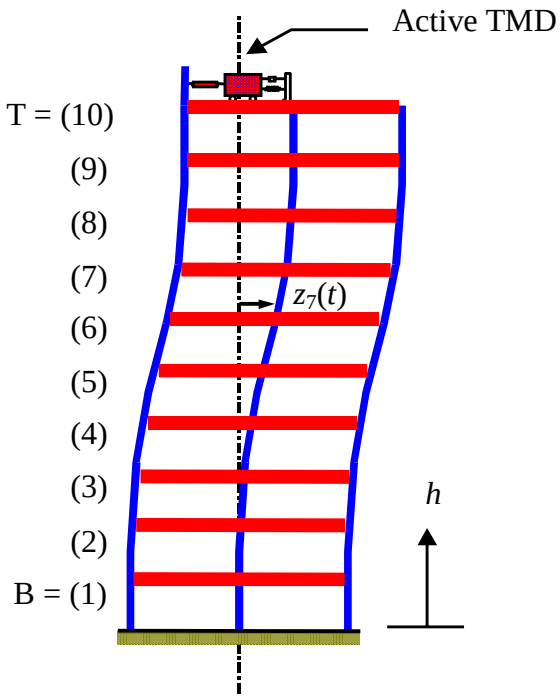


Figure 6-3: Schematic representation of a building equipped with an active TMD.

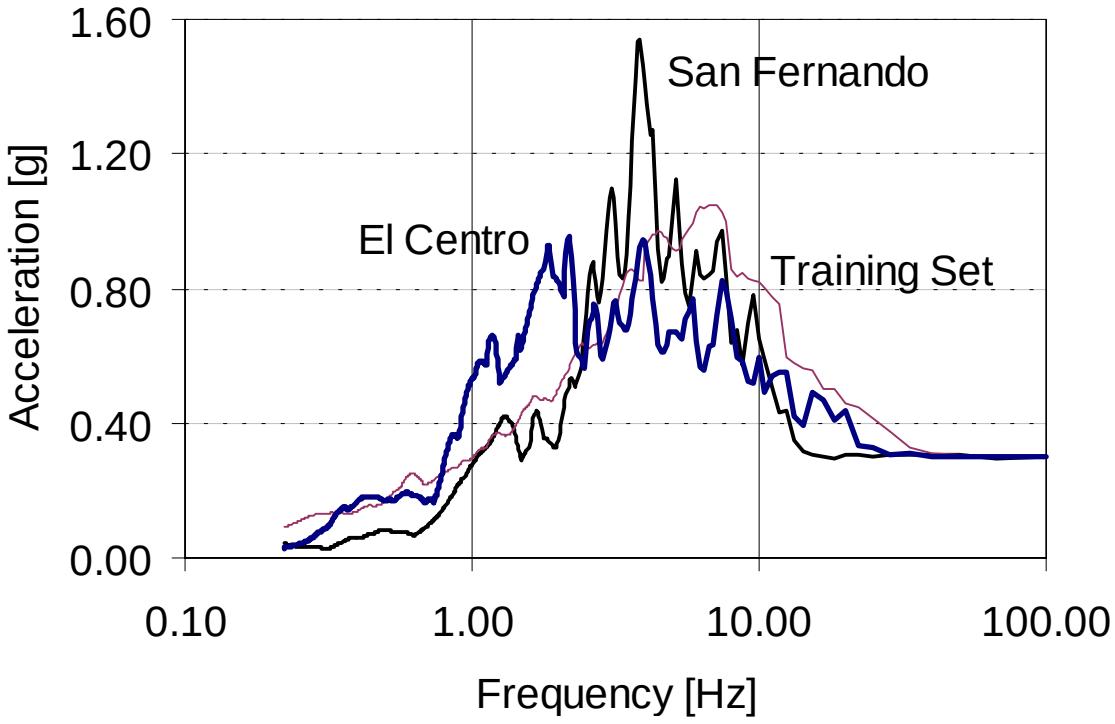


Figure 6-4: Response spectra of El Centro, San Fernando and the average of the training set earthquakes.

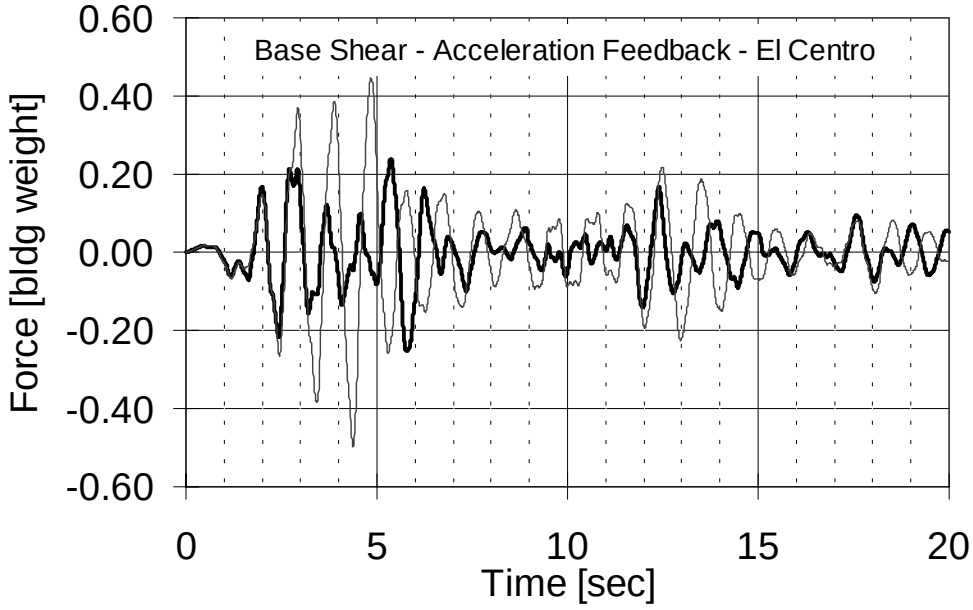


(a)

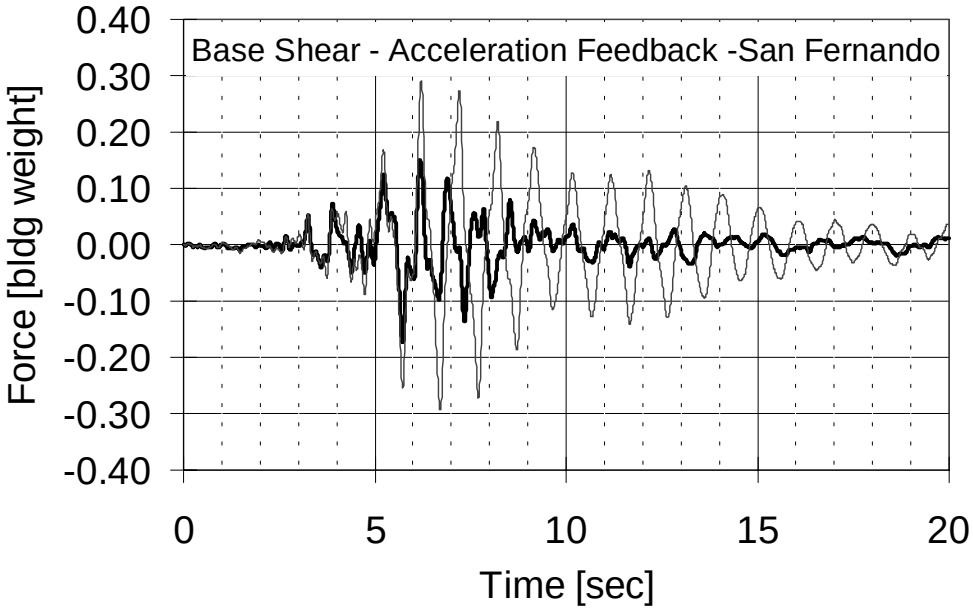


(b)

Figure 6-5: Comparison of uncontrolled and acceleration-feedback-control base shear responses for (a) El Centro motion and (b) San Fernando motion.

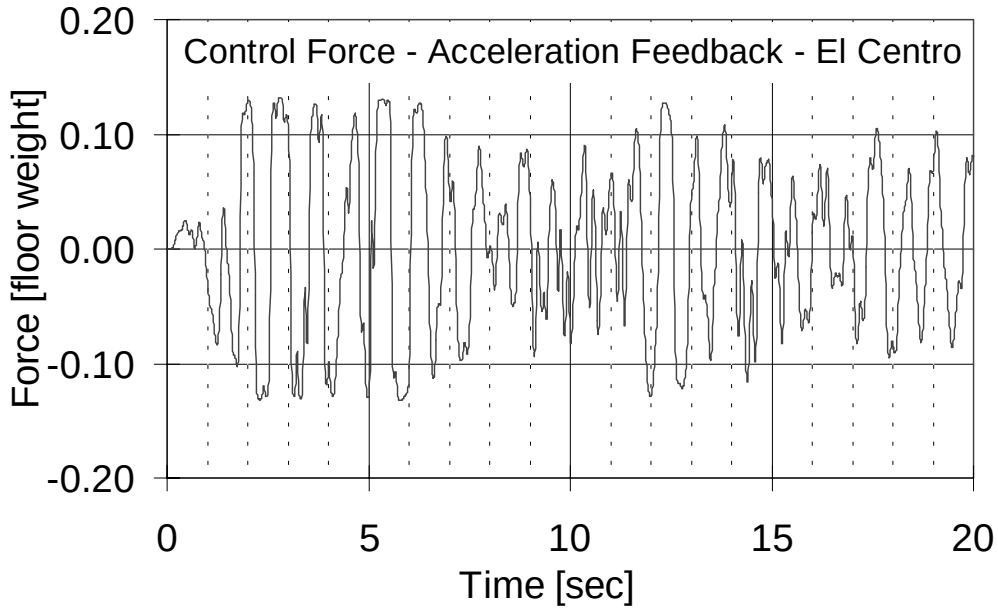


(a)

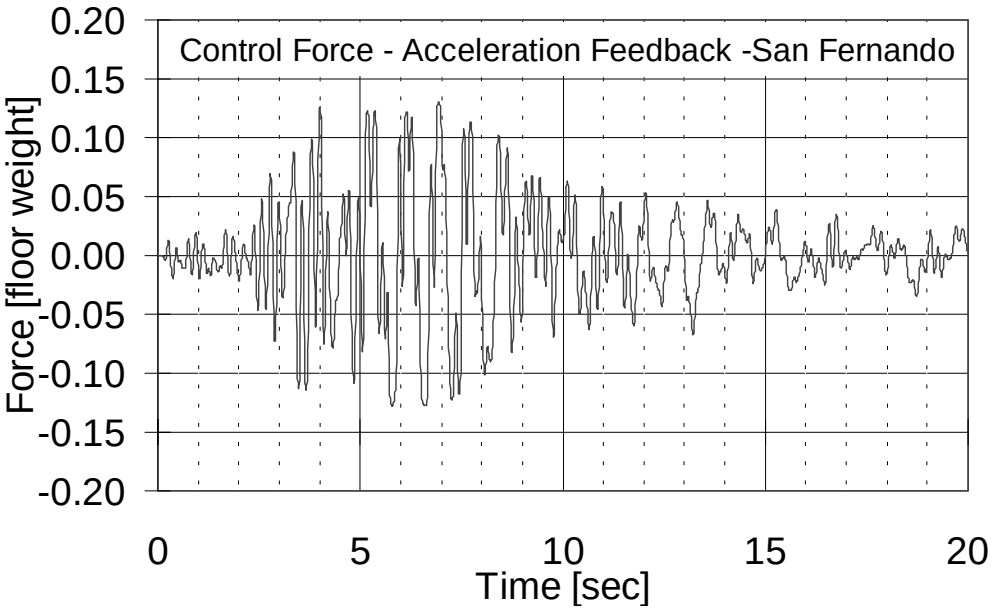


(b)

Figure 6-6: Control-force time histories for (a) El Centro motion and (b) San Fernando motion for acceleration feedback.

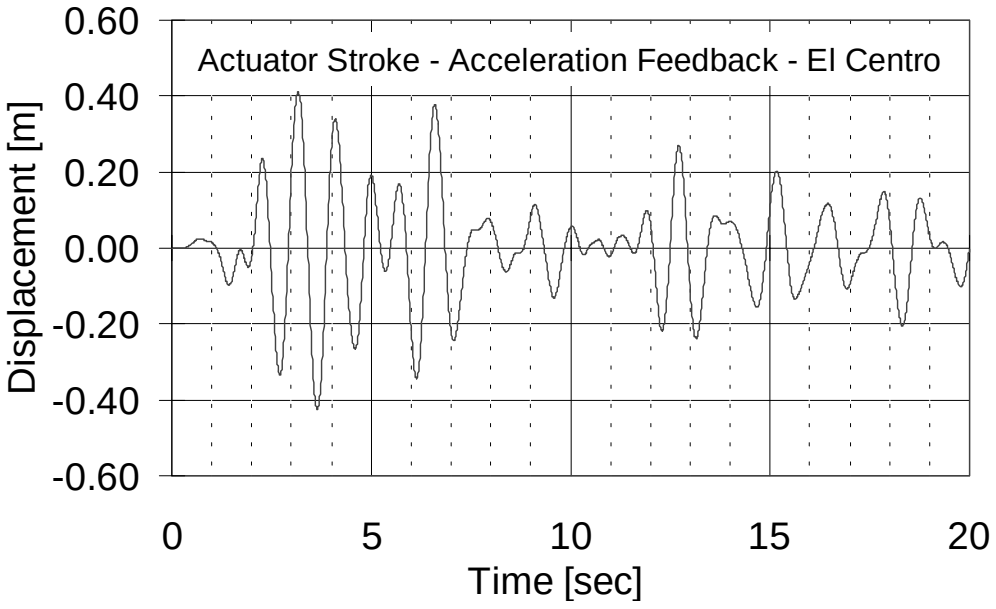


(a)

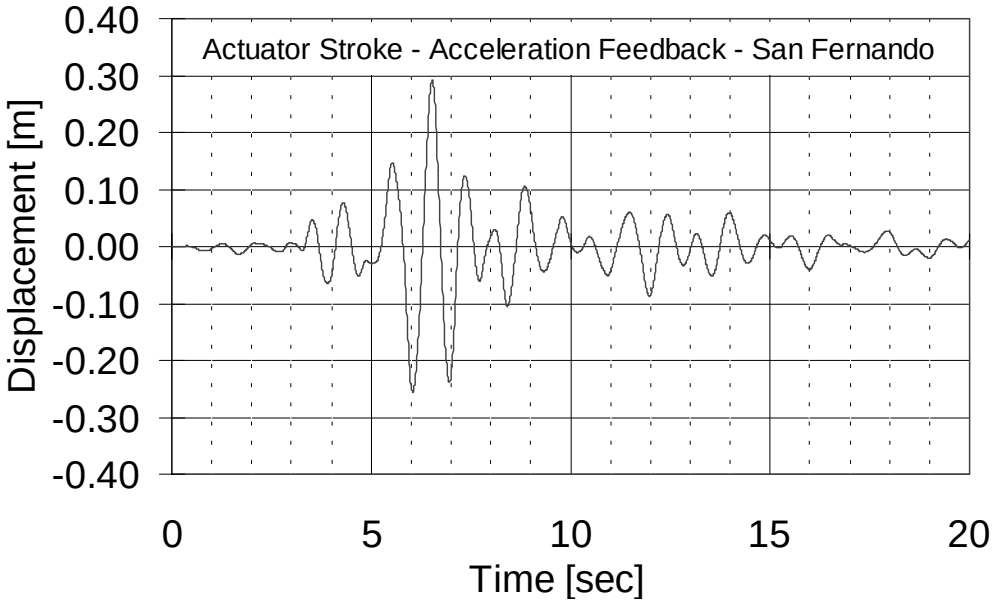


(b)

Figure 6-7: Actuator-stroke time histories for (a) El Centro motion and (b) San Fernando motion for acceleration feedback.

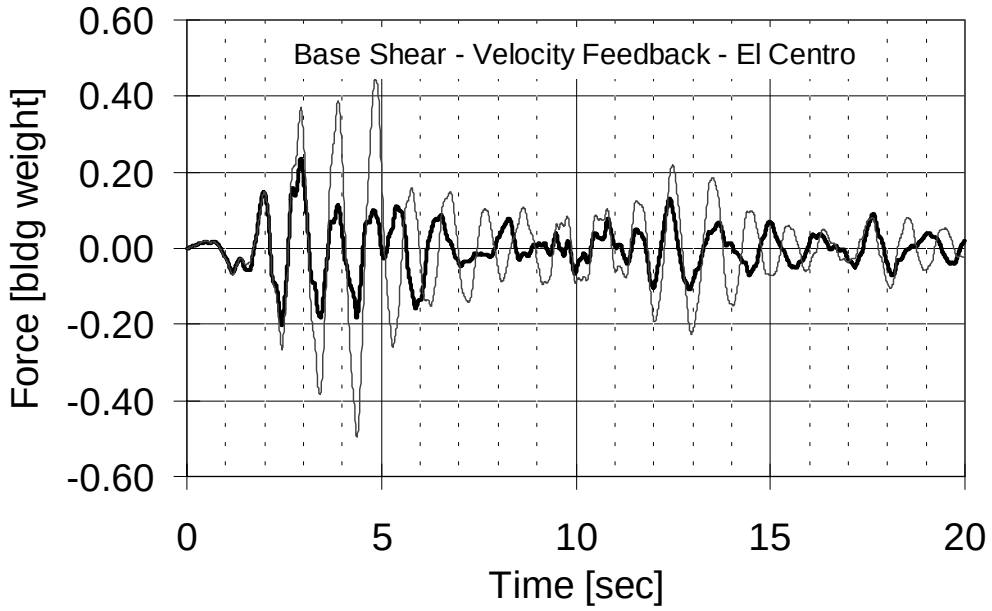


(a)

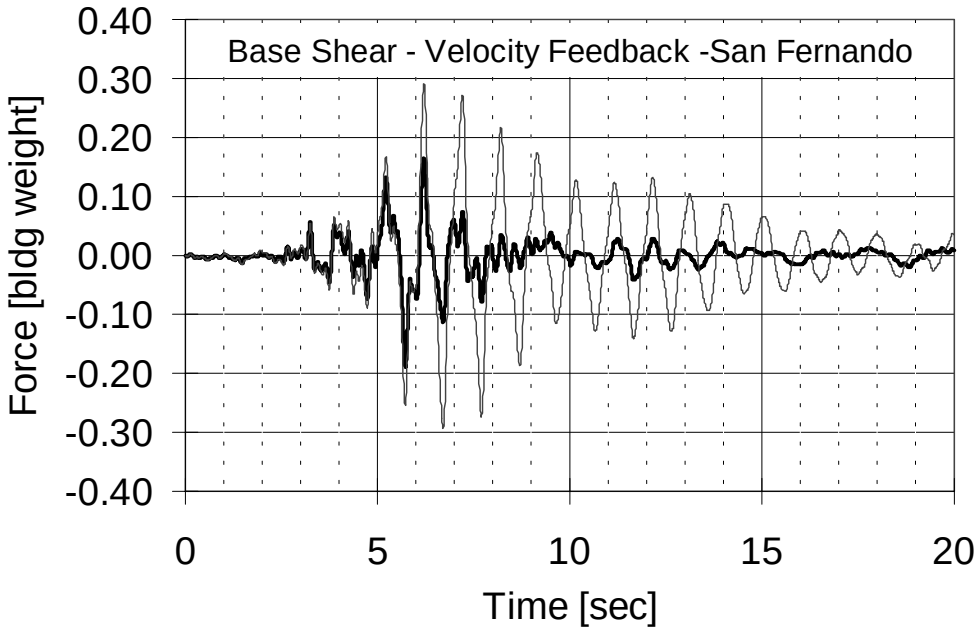


(b)

Figure 6-8: Comparison of uncontrolled and velocity-feedback-control base shear responses for (a) El Centro motion and (b) San Fernando motion.

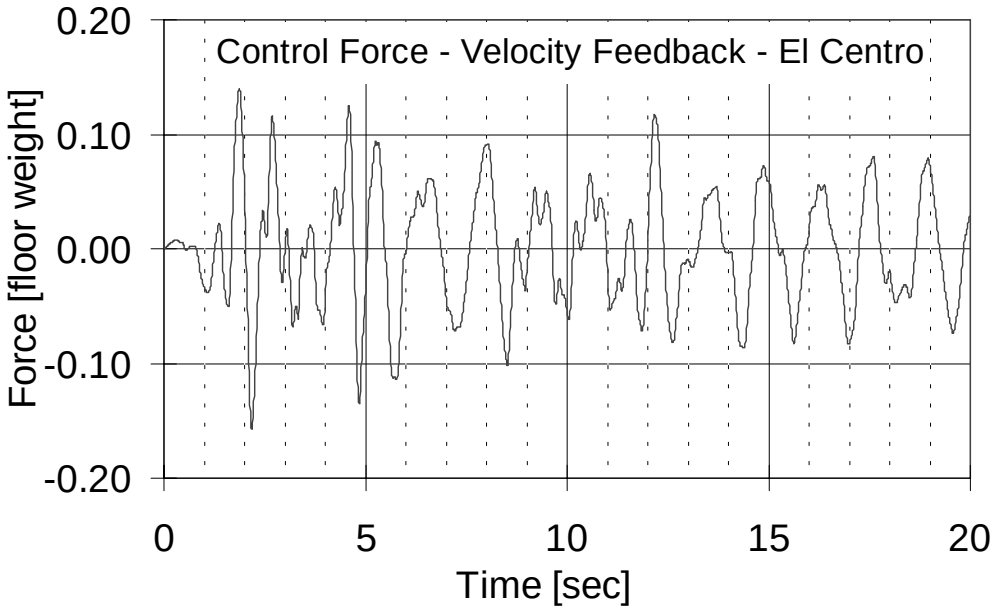


(a)

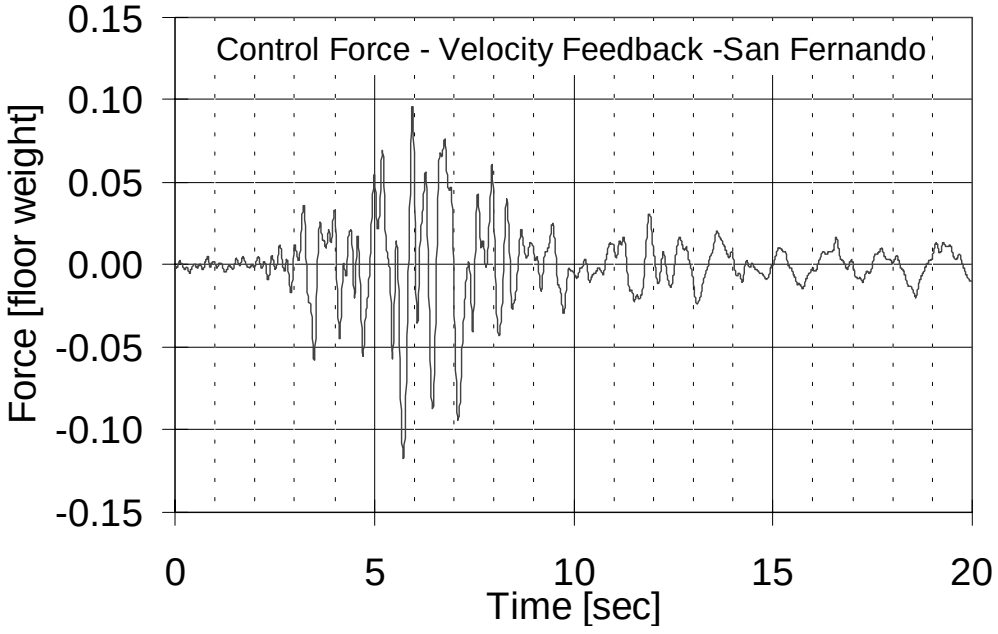


(b)

Figure 6-9: Control-force time histories for (a) El Centro motion and (b) San Fernando motion for velocity feedback.

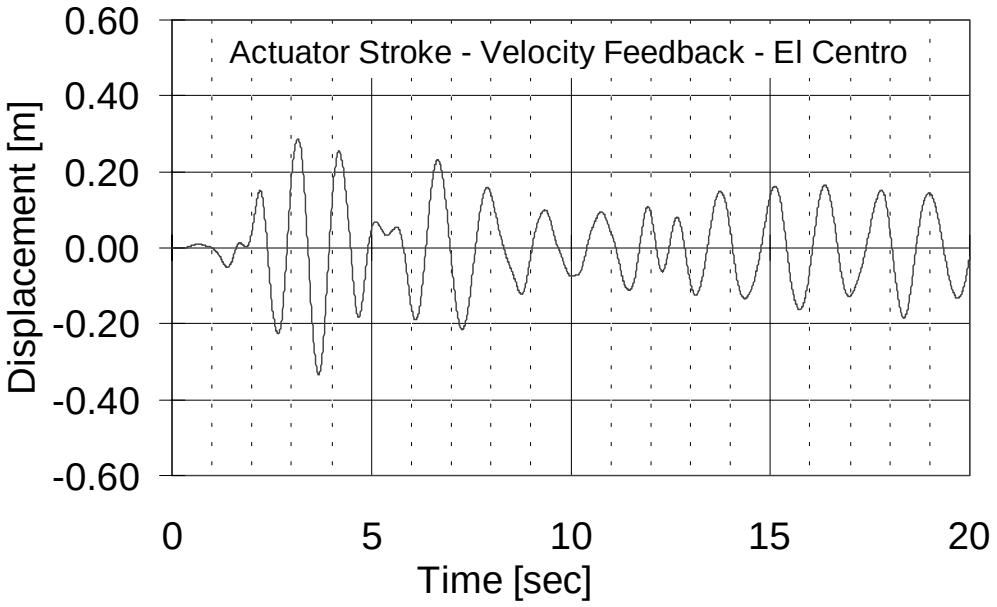


(a)

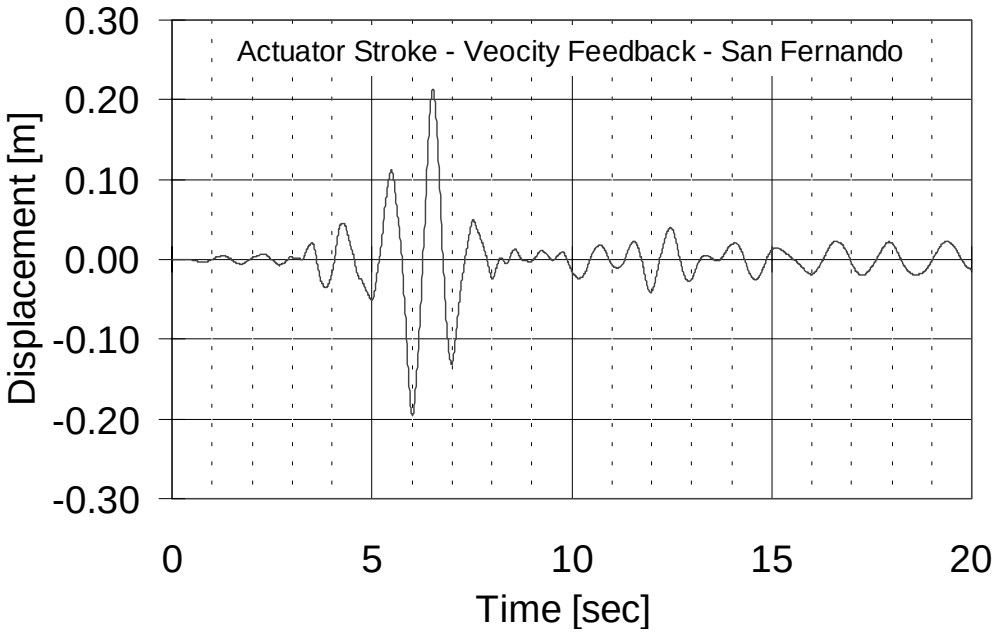


(b)

Figure 6-10: Actuator-stroke time histories for (a) El Centro motion and (b) San Fernando motion for velocity feedback.

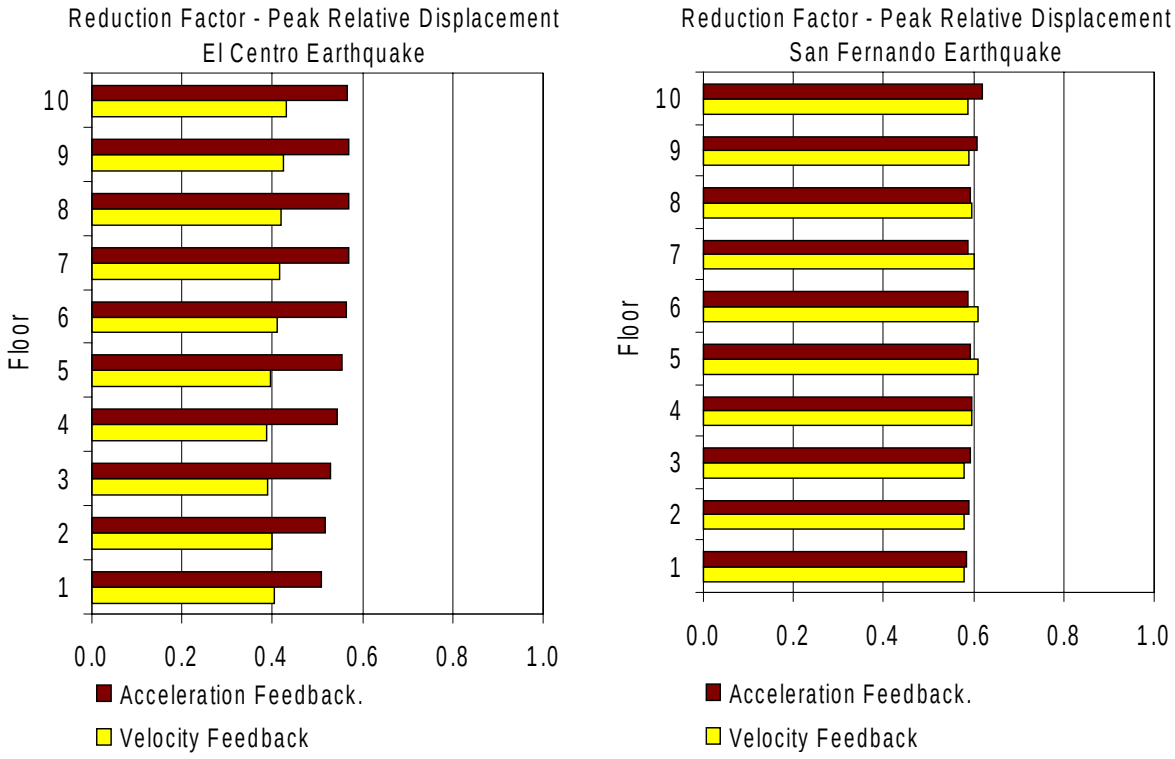


(a) (b)

Figure 6-11: Comparison of acceleration- and velocity-feedback peak relative displacement responses for (a) El Centro motion and (b) San Fernando motion. The results are normalized with the uncontrolled case.

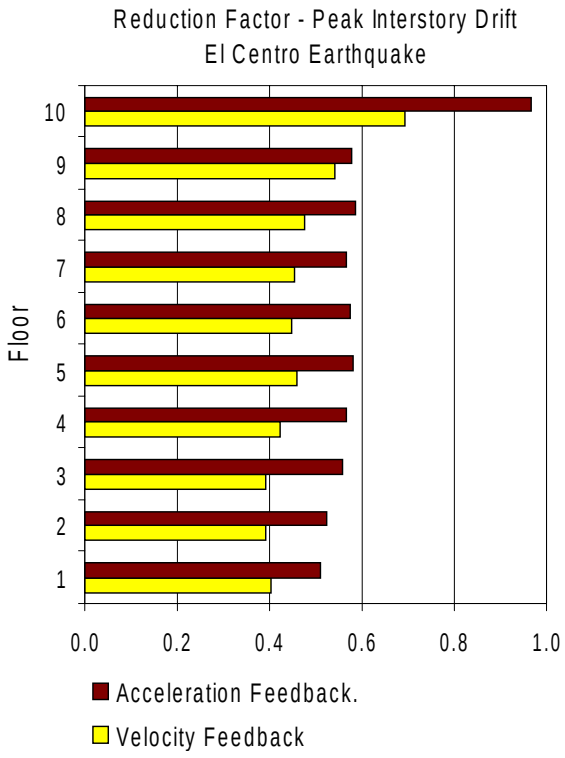


(a)

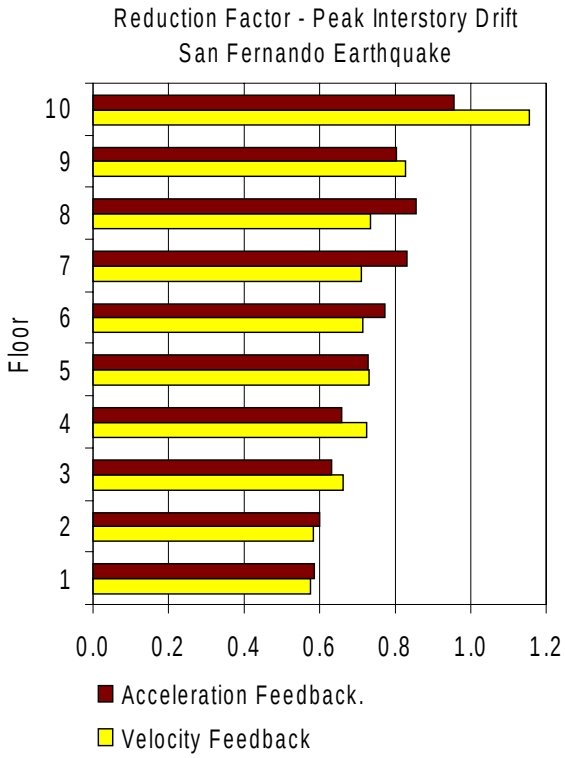


(b)

Figure 6-12: Comparison of acceleration- and velocity-feedback peak interstory drift responses for (a) El Centro motion and (b) San Fernando motion. The results are normalized with the uncontrolled case.

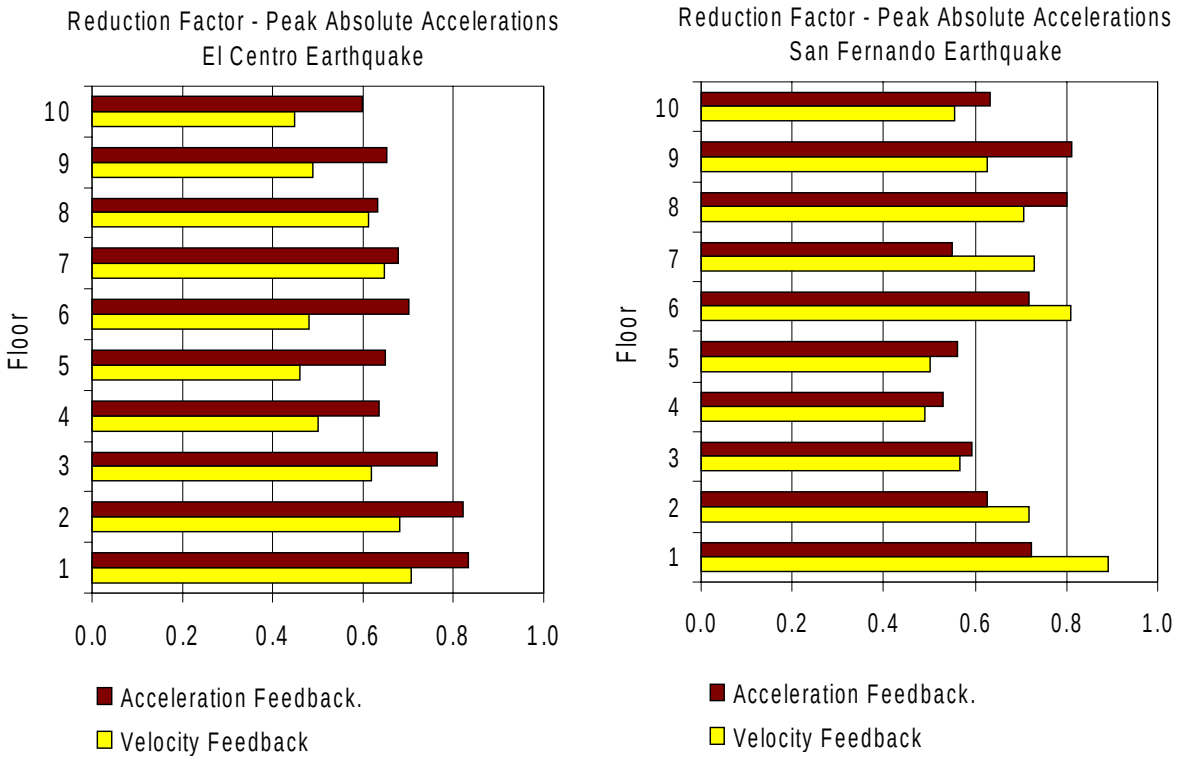


(a) (b)

Figure 6-13: Comparison of acceleration- and velocity-feedback peak absolute acceleration responses for (a) El Centro motion and (b) San Fernando motion. The results are normalized with the uncontrolled case.

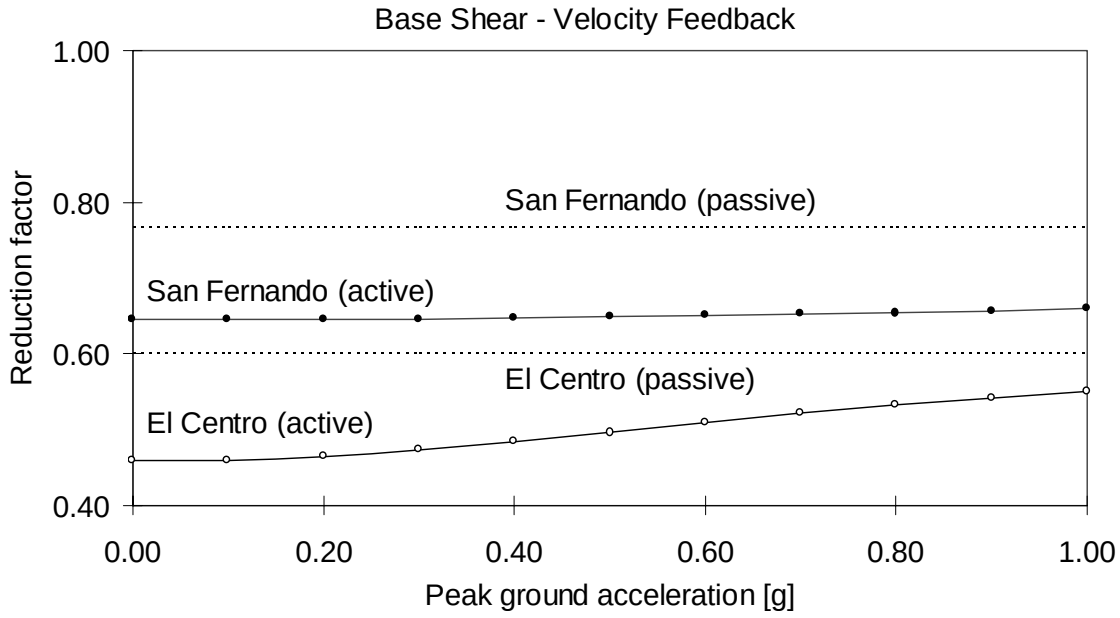


(a)

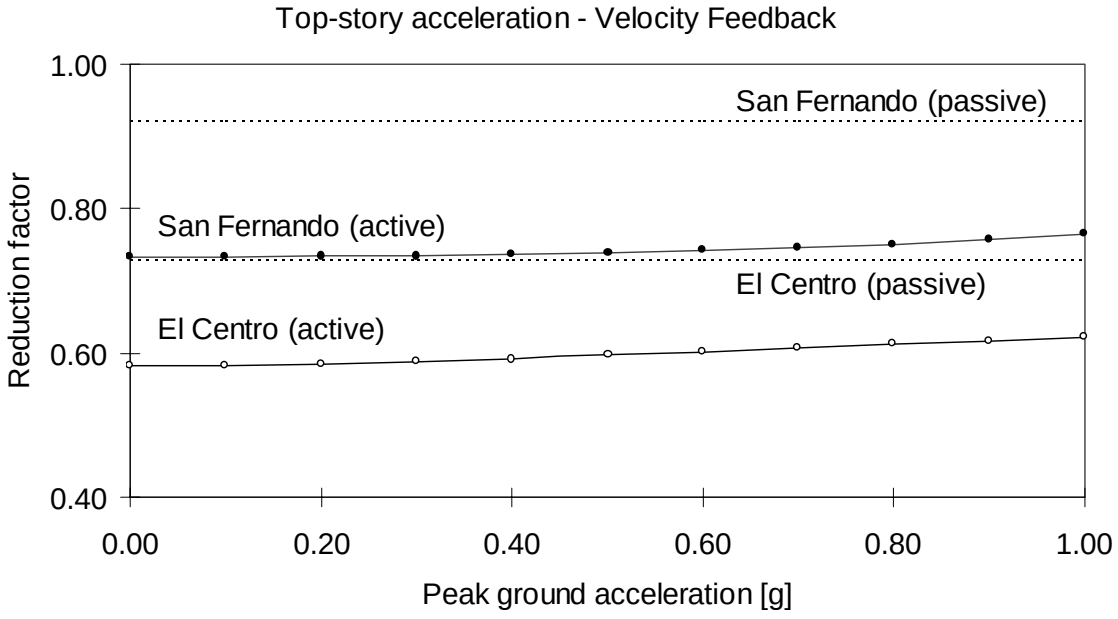


(b)

Figure 6-14: Response reduction for various levels of ground-motion intensities for (a) base shear and (b) top-floor accelerations for velocity feedback.

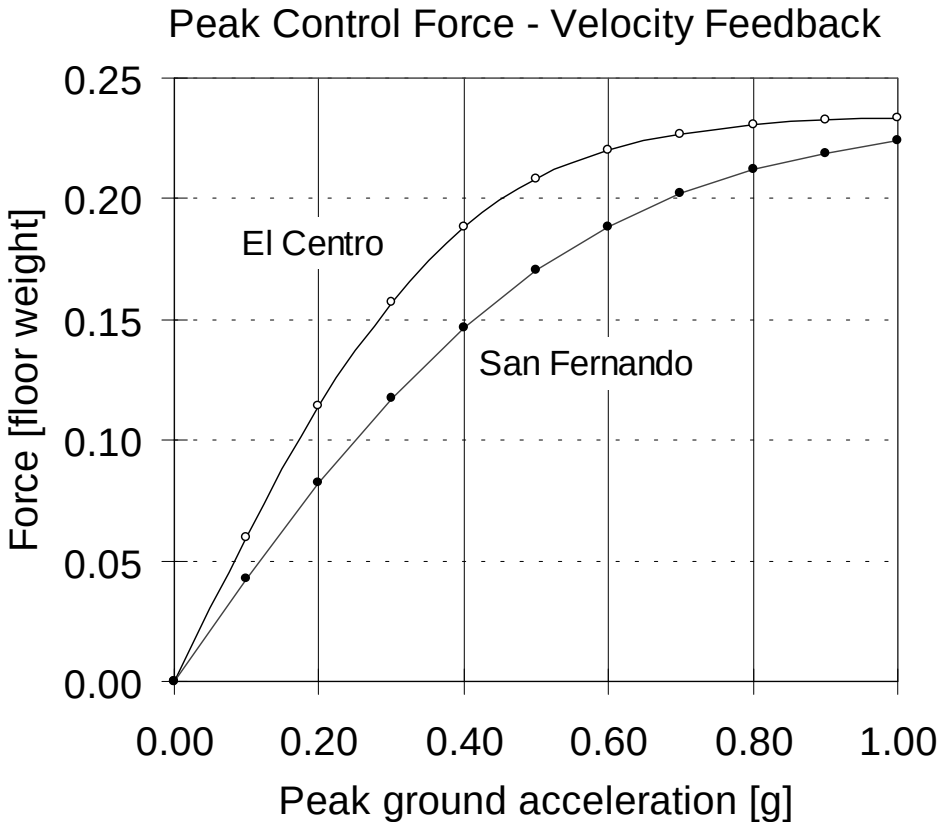


Figure 6-15: Nonlinear feature of the maximum control force required for various levels of ground-motion intensities for velocity feedback.

Table 6-1: Response ratios (of controlled to uncontrolled response) for El Centro and San Fernando earthquakes for various control schemes.

| | El Centro - 0.30 (*g*) | | | | | | | | |
|---|---|---|---|---|---|---|---|---|---|
| | **Relative Displacements** | | | **Interstorey Drifts** | | | **Absolute Accelerations** | | |
| Floor | **Passive** | **Accel. F.** | **Vel. F.** | **Passive** | **Accel. F.** | **Vel. F.** | **Passive** | **Accel. F.** | **Vel. F.** |
| 1 | 0.6030 | 0.5088 | 0.4038 | 0.6030 | 0.5088 | 0.4038 | 0.8935 | 0.8338 | 0.7070 |
| 2 | 0.5955 | 0.5170 | 0.3977 | 0.5859 | 0.5250 | 0.3901 | 1.0147 | 0.8213 | 0.6798 |
| 3 | 0.5866 | 0.5296 | 0.3913 | 0.5687 | 0.5584 | 0.3922 | 0.9075 | 0.7639 | 0.6180 |
| 4 | 0.5774 | 0.5439 | 0.3881 | 0.5914 | 0.5672 | 0.4227 | 0.6749 | 0.6359 | 0.5000 |
| 5 | 0.5714 | 0.5563 | 0.3964 | 0.6725 | 0.5806 | 0.4584 | 0.7749 | 0.6482 | 0.4588 |
| 6 | 0.5799 | 0.5640 | 0.4092 | 0.6947 | 0.5733 | 0.4478 | 0.6521 | 0.6998 | 0.4798 |
| 7 | 0.5981 | 0.5684 | 0.4175 | 0.6747 | 0.5670 | 0.4533 | 0.8297 | 0.6777 | 0.6463 |
| 8 | 0.6089 | 0.5684 | 0.4196 | 0.6493 | 0.5872 | 0.4768 | 0.8749 | 0.6313 | 0.6134 |
| 9 | 0.6161 | 0.5681 | 0.4239 | 0.6688 | 0.5779 | 0.5409 | 0.7356 | 0.6509 | 0.4893 |
| 10 | 0.6193 | 0.5664 | 0.4295 | 0.6442 | 0.9668 | 0.6937 | 0.7287 | 0.5990 | 0.4485 |

| | San Fernando - 0.30 (*g*) | | | | | | | | |
|---|---|---|---|---|---|---|---|---|---|
| | **Relative Displacements** | | | **Interstorey Drifts** | | | **Absolute Accelerations** | | |
| Floor | **Passive** | **Accel. F.** | **Vel. F.** | **Passive** | **Accel. F.** | **Vel. F.** | **Passive** | **Accel. F.** | **Vel. F.** |
| 1 | 0.7698 | 0.5850 | 0.5773 | 0.7698 | 0.5850 | 0.5773 | 1.0017 | 0.7240 | 0.8928 |
| 2 | 0.7742 | 0.5904 | 0.5768 | 0.7729 | 0.5986 | 0.5823 | 0.9523 | 0.6266 | 0.7179 |
| 3 | 0.7678 | 0.5913 | 0.5771 | 0.7509 | 0.6294 | 0.6622 | 0.9231 | 0.5919 | 0.5679 |
| 4 | 0.7492 | 0.5966 | 0.5949 | 0.8139 | 0.6583 | 0.7238 | 0.9121 | 0.5294 | 0.4911 |
| 5 | 0.6952 | 0.5926 | 0.6088 | 0.8894 | 0.7291 | 0.7312 | 0.8846 | 0.5601 | 0.5005 |
| 6 | 0.6940 | 0.5877 | 0.6095 | 0.9304 | 0.7713 | 0.7139 | 0.8836 | 0.7173 | 0.8094 |
| 7 | 0.6966 | 0.5881 | 0.6024 | 0.9542 | 0.8300 | 0.7092 | 0.8449 | 0.5500 | 0.7280 |
| 8 | 0.7028 | 0.5928 | 0.5948 | 0.9749 | 0.8561 | 0.7356 | 0.9242 | 0.8000 | 0.7055 |
| 9 | 0.7156 | 0.6064 | 0.5893 | 0.9292 | 0.8029 | 0.8261 | 0.9367 | 0.8111 | 0.6282 |
| 10 | 0.7271 | 0.6196 | 0.5857 | 0.9127 | 0.9560 | 1.1545 | 0.9233 | 0.6327 | 0.5550 |